JACS
JOURNAL OF THE AMERICAN CHEMICAL SOCIETY
Article
pubs.acs.org/JACS

Influence of Surface Adsorption on the Oxygen Evolution Reaction on $IrO_2(110)$

Ding-Yuan Kuo,[†] Jason K. Kawasaki,[‡,§,⊥] Jocienne N. Nelson,[‡] Jan Kloppenburg,[∥] Geoffroy Hautier,[∥] Kyle M. Shen,[‡,§] Darrell G. Schlom,[†,§] and Jin Suntivich*[,†,§]

[†]Department of Materials Science and Engineering, Cornell University, Ithaca, New York 14853, United States
[‡]Laboratory of Atomic and Solid State Physics, Department of Physics, Cornell University, Ithaca, New York 14853, United States
[§]Kavli Institute at Cornell for Nanoscale Science, Ithaca, New York 14853, United States
[∥]Institute of Condensed Matter and Nanosciences (ICMN), Université catholique de Louvain, Louvain-la-Neuve 1348, Belgium

Supporting Information

ABSTRACT: A catalyst functions by stabilizing reaction intermediates, usually through surface adsorption. In the oxygen evolution reaction (OER), surface oxygen adsorption plays an indispensable role in the electrocatalysis. The relationship between the adsorption energetics and OER kinetics, however, has not yet been experimentally measured. Herein we report an experimental relationship between the adsorption of surface oxygen and the kinetics of the OER on $IrO_2(110)$ epitaxially grown on a $TiO_2(110)$ single crystal. The high quality of the IrO_2 film grown using molecular-beam epitaxy affords the ability to extract the surface oxygen adsorption and its impact on the OER. By examining a series of electrolytes, we find that the adsorption energy changes linearly with pH, which we attribute to the electrified interfacial water. We support this hypothesis by showing that an electrolyte salt modification can lead to an adsorption energy shift. The dependence of the adsorption energy on pH has implications for the OER kinetics, but it is not the only factor; the dependence of the OER electrocatalysis on pH stipulates two OER mechanisms, one operating in acidic solution and another operating in alkaline solution. Our work points to the subtle adsorption−kinetics relationship in the OER and highlights the importance of the interfacial electrified interaction in electrocatalyst design.

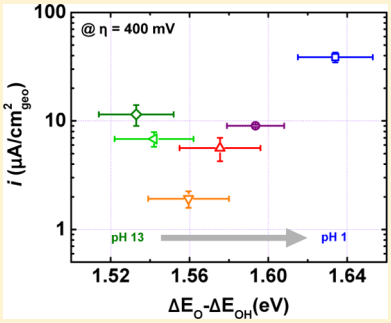

INTRODUCTION

The sluggish kinetics of the oxygen evolution reaction (OER) (acidic: $2H_2O \rightarrow O_2 + 4H^+ + 4e^-$; alkaline: $4OH^- \rightarrow O_2 + 2H_2O + 4e^-$) currently limits the efficiency of a water electrolysis device.[1−4] Many researchers have attributed the sluggish OER kinetics to the unfavorable formation energies of the intermediates,[5−7] which must be facilitated by overpotential. The function of an electrocatalyst is to stabilize these intermediates by reducing their energies while ensuring that their desorption step is not so overly energy-intensive (i.e., the volcano relation or the Sabatier principle[8]) that it becomes a new source of inefficiency. In this framework, the most active electrocatalyst is a material whose surface−oxygen interaction is neither too strong nor too weak.

The surface−oxygen adsorption energy is, however, difficult to assess experimentally, especially for transition-metal oxides, whose polar surfaces may electrostatically interact with nearby molecules in the presence of an electrochemical potential.[9] As a result, many researchers have attempted to create useful approximations. Examples include the work by Trasatti,[10] who used the enthalpy from a lower to higher oxide transition, Shao-Horn and co-workers, who used molecular-orbital principles,[11] and Nørskov and Rossmeisl, who used density functional theory (DFT) calculations to approximate the surface−oxygen adsorption energy.[12] In the past decade, this computational approach has been used to explore cation substitutions,[13−15] strain tuning,[16] and structural engineering[17−20] for oxide electrocatalyst design. These investigations have shown that the surface−oxygen interaction energy is centrally important.

While these "descriptor" approaches have led to the discovery of highly active OER electrocatalysts,[6,14,21] they often assume a vacuum surface model. Although computationally the presence of water molecules weakly affects the surface adsorption energy on platinum,[22] recent experiments by Yan and co-workers[23,24] and Koper and co-workers[25,26] have shown that the electrolyte and water *can* influence the surface adsorption energy on platinum. As most OER electrocatalysts are oxides with polar surfaces,[27,28] the surface interaction with the electrolyte and water could be even stronger. These considerations thus beckon the question of how the calculated energies of intermediates (OH_{ad}, O_{ad}, and OOH_{ad}) on oxide surfaces[7] compare to values from experiments in the presence of both an electrolyte and an electrochemical potential. Unfortunately, there is not yet a report on the experimental surface−oxygen interaction energy, especially on IrO_2, a common standard for a stable, active OER electrocatalyst. As

Received: November 18, 2016
Published: February 9, 2017

DOI: 10.1021/jacs.6b11932
J. Am. Chem. Soc. 2017, 139, 3473−3479

a result, it is still unclear whether the approximations (i.e., neglecting the interfacial water layer and the surface work function constraint[29]) are appropriate.

Single crystals offer an unprecedented window to examine these surface processes. Surface adsorption energies for Pt(*hkl*)[30−33] have been used to benchmark DFT calculations[34,35] by using H_{ad} and OH_{ad} electroadsorption from cyclic voltammetry (CV) to validate the calculated adsorption energies. These efforts have led to the development of successful catalysts such as $Pt_3Ni(111)$[36] and Pt_3Y.[37] In oxides, however, this comparison is not straightforward because of the limited availability of oxide single crystals. Notably, the high melting point and concern over impurities make the process of synthesizing single-crystal oxides highly time-consuming and enormously complex.[38] Still, a few research groups have managed to conduct fundamental electrochemistry studies on conductive single-crystal oxides. Examples include O'Grady and co-workers, whose works have investigated surface adsorption on several RuO_2 single-crystal facets.[39−41] Similar work has been done on IrO_2.[42] Nevertheless, the connection between the surface−oxygen interaction and OER electrocatalysis remains to be made.

To investigate the linkage between surface adsorption and OER electrocatalysis, we used molecular-beam epitaxy (MBE) to grow single-crystal $IrO_2(110)$ as a model oxide surface. Recent advances in oxide synthesis using thin-film deposition methods have enabled unprecedented access to electrochemistry on single crystals prepared in thin-film form. Many researchers have taken advantage of these atomically precise oxide films to reveal the orientation dependence of electrocatalysis on RuO_2 and IrO_2[43] as well as the effects of strain[16] and resistance[44] on the OER kinetics. In this work, we focus on rutile $IrO_2(110)$ films grown on single-crystal rutile $TiO_2(110)$ substrates to avoid the possibility of twin boundary formation (due to multiple positioning on substrates that are not isostructural) or faceting.

In this contribution, we describe our measurement of the surface−oxygen electroadsorption energy on IrO_2 films epitaxially grown on TiO_2 single-crystal substrates. We seek to address the surface−oxygen interaction by investigating the adsorption of OH_{ad} and O_{ad} on single-crystal $IrO_2(110)$ and examining the influence of the electrolyte. Finally, we connect these adsorption results with the OER electrocatalysis.

EXPERIMENTAL SECTION

Molecular-Beam Epitaxy Synthesis. $IrO_2(110)$ films were grown by MBE on single-crystal $TiO_2(110)$ using a distilled ozone oxidant at a background pressure of 10^{-6} Torr. The flux of iridium was initially calibrated using a quartz crystal microbalance. The epitaxial nature of the as-grown films was confirmed by in situ reflection high-energy electron diffraction (RHEED), low-energy electron diffraction (LEED), and X-ray diffraction (XRD) (Rigaku SmartLab). Further growth details can be found in Ref 55.

Preparation of Electrolytes. The 0.1 M perchloric acid ($HClO_4$), 0.1 M potassium phosphate monobasic (KH_2PO_4), 0.1 M potassium phosphate dibasic (K_2HPO_4), 0.1 M potassium hydrogen carbonate ($KHCO_3$), 0.1 M potassium carbonate (K_2CO_3), and 0.1 M potassium hydroxide (KOH) solutions were prepared by dissolving $HClO_4$ (with concentration 70%, EMD), KH_2PO_4 (99.995% purity, Sigma-Aldrich), K_2HPO_4 (99.95% purity, Sigma-Aldrich), $KHCO_3$ (99.7−100.5% (dried basis), Alfa Aesar), K_2CO_3 (99.997% purity, Alfa Aesar), and KOH pellets (99.99% purity, Sigma-Aldrich) in deionized water (18.2 MΩ cm). The pH 2.8 phosphate buffer, pH 6.5 phosphate buffer, and pH 9.6 carbonate buffer were prepared by adding 0.1 M $HClO_4$ to 0.1 M KH_2PO_4, 0.1 M KH_2PO_4 to 0.1 M K_2HPO_4, and 0.1 M $KHCO_3$ to 0.1 M K_2CO_3.

The pH values of the electrolytes were calculated from the H_2/H^+ equilibrium potential (vs Ag/AgCl). At the zero-current potential, the pH values satisfy the Nernst equation:

$$E_{H_2/H^+}\ (\text{vs Ag/AgCl}) = -E_{Ag/AgCl} - \frac{2.303RT}{F}\text{pH}$$

Electrochemical Characterization. Electrical contacts were made using the same protocol as reported previously.[43] Briefly, titanium wires were attached to IrO_2 films using silver paint (Leitsilber 200, Ted Pella), and the samples were covered with epoxy (Omegabond 101) except for the IrO_2 films. All electrochemical characterization was conducted in a three-electrode glass cell with a potentiostat (Bio-Logic). The reference electrode was a Ag/AgCl redox couple in a saturated KCl solution, calibrated to the H_2 redox potential. The counter electrode was a Pt wire. The electrolyte/cell-resistance-corrected potential was obtained by correcting the potential with the electrolyte/cell resistance as determined using the high-frequency intercept of the real resistance from an impedance measurement. First, we conducted CV in Ar-saturated electrolytes at a scan rate of 200 mV/s to observe surface adsorption. To avoid the large capacitance current, the OER measurement was conducted in O_2-saturated electrolytes at a scan rate of 10 mV/s. Capacitance-free CV curves were obtained by averaging the forward and backward scans.

Computations. The van der Waals-corrected[45] RPBE functional[46] was used for all computations. Our slab model consisted of a four-trilayer hydrogen-terminated slab. The two bottom layers were fixed at the bulk positions, while the two top layers, including adsorbates, were allowed to fully relax. This choice of functional and slab configuration is consistent with the work of other groups.[6,7,47] The criterion for a converged geometry was set to achieve all forces below 0.01 eV/Å, and we used an 8 × 4 × 1 Γ-centered **k**-point grid for slab computations. Our slab model had two coordinatively unsaturated sites (cus). For VASP[48−50] computations, a minimum vacuum distance of 15 Å was ensured, while structures for FHI-AIMS[51] computations had a minimum of 80 Å separating the slab images. Total energy computations were performed with the all-electron code FHI-AIMS employing the default *tight* basis sets.[51] In addition to zero-point energies (ZPEs), we included solvation energy effects. Both ZPE and solvation energies were computed with VASP using the PAW pseudopotentials.[52] ZPEs for adsorbed molecules were computed with a 400 eV plane-wave cutoff, and solvation energies were computed with the cutoff set to 800 eV and the dielectric constant set to 78.4 for water. The energetically most stable structures and transition energies for adsorbates on the catalyst were determined by a surface theoretical approach. The main difference compared with the standard Norskov/Rossmeisl approach is that in our model the catalytically active Ir binding sites in starting geometries were saturated with water molecules, and we also employed an implicit solvation model as implemented by VASPsol.[53,54] We did not include any explicit molecular water layers in addition to surface adsorbates.

RESULTS AND DISCUSSION

In Figure 1 we show the θ−2θ X-ray diffraction scan of $IrO_2(110)$ (Figure 1a) in combination with its LEED image (Figure 1b), which verify the epitaxial nature of the IrO_2 film. The RHEED pattern measured during the growth shows a sharp and streaky pattern, which demonstrates the high quality of the IrO_2 single crystal film (Figure S1). In situ RHEED and both on- and off-axis X-ray diffraction scans indicate that the $IrO_2(110)$ film is partially relaxed at the synthesized thickness (~8 nm) used in this work. We have previously shown that the electronic structure of the $IrO_2(110)$ film closely matches that of the bulk structure;[55] we therefore do not anticipate strain to play a major role here. Finally, we used LEED to verify the (110) termination of the synthesized IrO_2 film (Figure 1b).

DOI: 10.1021/jacs.6b11932
J. Am. Chem. Soc. 2017, 139, 3473−3479

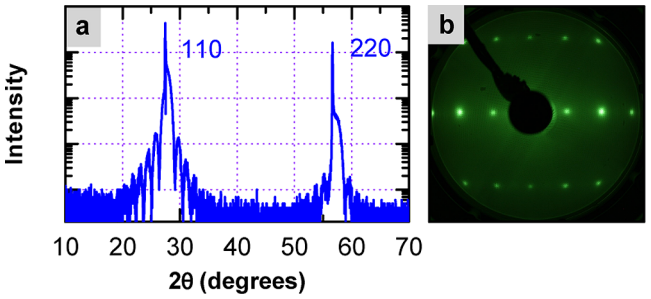

Figure 1. (a) θ–2θ X-ray diffraction scan of an epitaxial IrO_2 film (20 formula units thick) grown on a single-crystal $TiO_2(110)$ substrate. (b) LEED pattern recorded from $IrO_2(110)/TiO_2(110)$.

We examined surface adsorption on the $IrO_2(110)$ film using CV techniques. In Figure 2a, the CV curve for $IrO_2(110)$ in 0.1 M KOH shows peaks at ~0.9 V vs reversible hydrogen electrode (RHE) (peak 1) and ~1.5 V vs RHE (peak 2). Similar CV curves have been reported on a rutile $IrO_2(110)$ thin film[43] and amorphous films.[56] Integrating the charge under the CV curve suggests that only surface Ir participates in the electron transfer (67.8 $\mu C/cm^2$ without double-layer correction, corresponding to 0.85 electron per surface coordinately undersaturated Ir (Ir_{cus}) site; Figure S2). We note that the CV peaks for IrO_2 have been assigned as the redox peaks for Ir,[57−59] which are analogous to the surface electroadsorption/desorption.

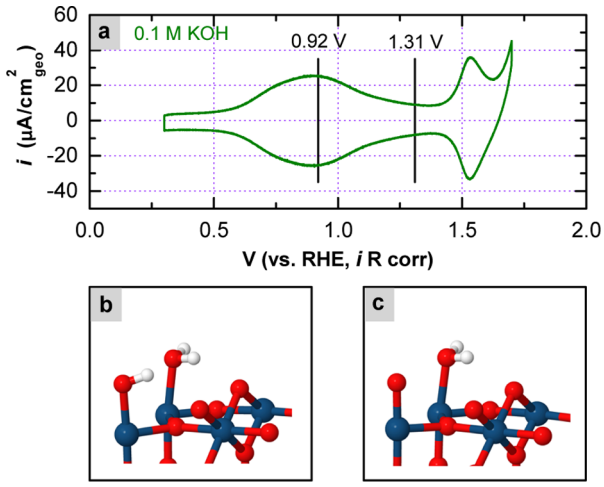

Figure 2. (a) Cyclic voltammogram of $IrO_2(110)$ in Ar-saturated 0.1 M KOH at a scan rate of 200 mV/s. The solid lines are OH_{ad} and O_{ad} binding energies from our DFT calculations. (b) OH_{ad} and (c) O_{ad} adsorption models for our DFT calculations.

To verify the nature of these adsorptions, we used DFT calculation to assess the binding energies for OH_{ad} and O_{ad} on Ir_{cus}. The peak energies of OH_{ad} and O_{ad} on Ir_{cus} are 0.92 and 1.31 V vs computational hydrogen electrode (a theoretical analogue of the RHE), respectively (solid lines in Figure 2a). Although these results do not exactly match the CV results, they provide us with confidence in the assignments that peak 1 is likely due to OH_{ad} adsorption and peak 2 to O_{ad} adsorption. We note that the broad and narrow peak widths in peaks 1 and 2, respectively, are consistent with strong near-neighbor interactions in OH_{ad} in comparison with O_{ad}.[60] The difference in the calculated and measured OH_{ad} and O_{ad} adsorption energies on IrO_2 could be due to the presence of electrolyte (e.g., water) near the IrO_2 surface. The role of the interfacial electrolyte is shown through the role of pH on the adsorption of OH_{ad} and O_{ad}. We observe that the adsorption peaks shift to more positive potentials at lower pH (Figure 3a), highlighting how changing the electrolyte can affect the OH_{ad} and O_{ad} adsorption energies. We note that the direction of change of the pH dependence is the same as for an oxidized iridium metal electrode,[61] a hydrous IrO_2 film,[62] and the OH_{ad} adsorption on platinum.[23]

To quantify this pH dependence, we used the potential at the adsorption peak (V_{peak}), which corresponds to the half-coverage potential, and the potential window at 90% peak current as error bars in Figure 3b to demonstrate the peak width difference between OH_{ad} and O_{ad}. In this analysis, although both OH_{ad} and O_{ad} follow the same pH direction, their pH dependences have different slopes (25 and 7.5 mV/pH unit, respectively). One possible explanation of this observation is the pH dependence of the water structure at the interface, manifested as the work function shift with pH, as has been recently explored by Rossmeisl and co-workers to explain the anomalous pH shift in RuO_2 electrochemical features.[29] This non-Nernstian adsorption peak shift might also indicate that the adsorption and desorption processes have noninteger electron transfer.[63−65]

To estimate the free energy of formation of OH_{ad} and O_{ad} on IrO_2, we examine the potentials of OH_{ad} (acidic: $H_2O_{ad} \rightarrow OH_{ad} + H^+ + e^-$; alkaline: $H_2O_{ad} + OH^- \rightarrow OH_{ad} + H_2O + e^-$) and O_{ad} (acidic: $OH_{ad} \rightarrow O_{ad} + H^+ + e^-$; alkaline: $OH_{ad} + OH^- \rightarrow O_{ad} + H_2O + e^-$). The electrochemical potentials of OH_{ad} ($\Delta E_1 = V_{peak\ 1}$) and O_{ad} ($\Delta E_2 = V_{peak\ 1} + V_{peak\ 2}$) correspond to the free energies of $H_2O_{ad} \rightarrow OH_{ad} + {}^1/_2H_2$ and $H_2O_{ad} \rightarrow O_{ad} + H_2$, respectively (shown in Figure 3c). We observe that the free energy shifts of both OH_{ad} and O_{ad} with pH occur in a way that preserves the scaling relation (a linear relationship between

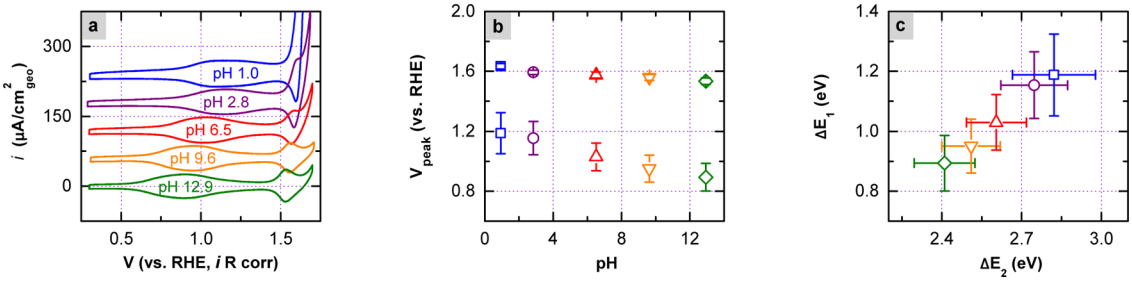

Figure 3. (a) Cyclic voltammograms of $IrO_2(110)$ in Ar-saturated 0.1 M electrolytes with different pH values at a scan rate of 200 mV/s. (b) Shifts of the adsorption peak potentials with pH from (a). (c) Energy relationship between the adsorbates for peaks 1 and 2 from (a).

DOI: 10.1021/jacs.6b11932
J. Am. Chem. Soc. 2017, 139, 3473−3479

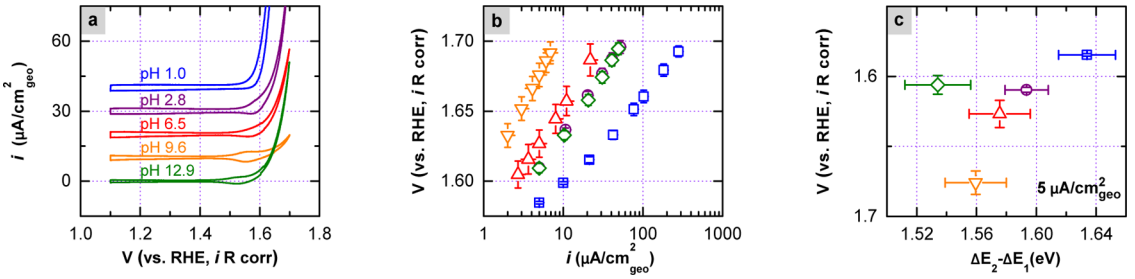

Figure 4. (a) Cyclic voltammograms of $IrO_2(110)$ in O_2-saturated 0.1 M electrolytes with different pH values at a scan rate of 10 mV/s. (b) Tafel plots for the OER kinetics of $IrO_2(110)$ at different pH values. (c) Overpotentials for the OER at 5 $\mu A/cm^2_{geo}$ at different pH values.

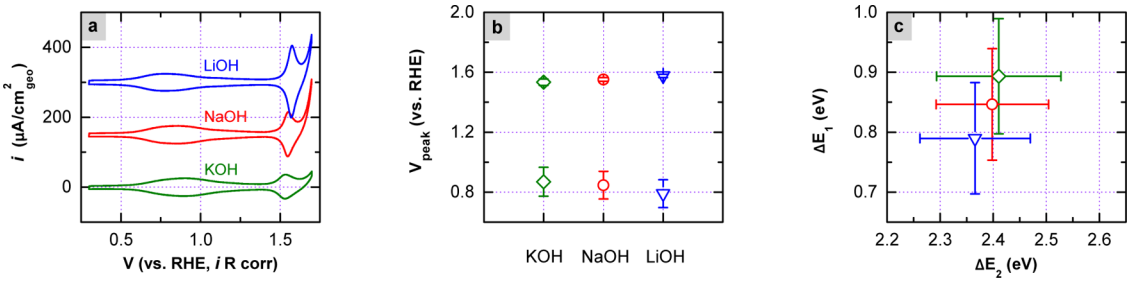

Figure 5. (a) Cyclic voltammograms of $IrO_2(110)$ in Ar-saturated 0.1 M KOH, NaOH, and LiOH at a scan rate of 200 mV/s. (b) Shifts of the adsorption peak potentials with the cation from (a). (c) Energy relationship between the adsorbates for peaks 1 and 2 from (a).

the OH_{ad} and O_{ad} free energies).[7,66] This observation suggests that the influence of the electric field at the interface on the surface bonding as a result of the work function shift may occur in a way that preserves the scaling relation. One possible explanation is that the electric field affects the dipole orientation of water, which in turn systematically modifies both the OH_{ad} and O_{ad} adsorption energies in a way that preserves the scaling relation.[29,67]

We next explored whether the OH_{ad} and O_{ad} shifts impact the OER electrocatalysis. We show the OER kinetics as a function of pH in Figure 4. Our $IrO_2(110)$ displays activity similar to that reported previously for an $IrO_2(110)$ film in 0.1 M KOH[43] but lower than that of IrO_2 nanoparticles,[68] which may be associated with imperfections in the IrO_2 nanoparticles. We observe that the OER activity depends on pH with the rank pH 1.0 > pH 2.8 ≈ pH 12.9 > pH 6.5 > pH 9.6. $IrO_2(110)$ is observed to be more active in 0.1 M $HClO_4$ (pH 1.0) than in 0.1 M KOH (pH 12.9), as shown by a higher current density in $HClO_4$ at constant applied potential (Figure 4b). This observation is similar to the observed OER activity on IrO_2 nanoparticles, which is 3 times higher in acidic media than in alkaline media.[68] Interestingly, we find that the activity for $IrO_2(110)$ increases monotonically as the pH of the electrolyte decreases, except for pH 12.9 (Figure 4c).

We explain the pH dependence for pH 1−10 using the concept of the potential-limiting step (assuming that the anion adsorption effect is negligible). As the OH_{ad} and O_{ad} adsorptions change with pH, the energy of the rate-limiting formation of the OOH_{ad} intermediate changes accordingly. Nørskov and Rossmeisl have suggested the free energy difference between the OH_{ad} and O_{ad} adsorptions as an approximation to the energy of the rate-limiting OOH_{ad} formation.[6] Figure 4c shows the result of this approximation. Notably, we see that the OER activity scales linearly with $\Delta E_2 - \Delta E_1$ at pH 1−10, suggesting that the pH dependence of the OER is due to the unfavorable formation of the OOH_{ad} intermediate with increasing pH.

However, the concept of the potential-limiting step fails to explain the increased OER activity at pH 12.9 in comparison with pH 9.6. Minguzzi et al.[69] observed a similar trend that IrO_2 has lower activity in neutral phosphate media compared with the activities in $HClO_4$ and NaOH, suggesting that the activity depends on the reaction mechanism, which varies with pH. We use this explanation to rationalize the observed OER trend. We consider the acid−base transition of OOH_{ad} formation[6,70] (acidic: $O_{ad} + H_2O \rightarrow OOH_{ad} + H^+ + e^-$; alkaline: $O_{ad} + OH^- \rightarrow OOH_{ad} + e^-$). In the first-order rate law approximation, this rate-limiting step is proton-independent in acidic media at constant overpotential ($k_{acid} = k_{0,acid}\theta_{ad}$). In alkaline media, however, another pathway using OH^- becomes possible because of the increased availability of OH^- ($k_{base} = k_{0,base}[OH^-]\theta_{ad}$; see the Supporting Information).

We hypothesize that the alkaline pathway has a higher rate constant than the acidic pathway ($k_{0,base} \gg k_{0,acid}$). In going from pH 10 to 13, the alkaline pathway (k_{base}) becomes dominant because of the availability of OH^-, despite the increasingly difficult formation of the OOH_{ad}. To verify this hypothesis, we measured the OER kinetics at pH 11.9, 12.5, and 12.9 (Figures S3 and S4). The observed OER kinetics at these basic pHs support our hypothesis. Hence, we propose that the OER, even with the same-rate limiting OOH_{ad} formation, can occur via two reaction pathways, one acidic and one alkaline, which compete against one another. This hypothesis, if true, would explain why the OER activity increases with decreasing pH in the low-pH region and with increasing pH in the high-pH region. This mechanistic assumption also suggests that the reaction order with respect to OH^- should be <1. Notably, OH^- influences the kinetics in two ways: the first is via the first-order dependence on OH^- to affect k_{base}, and the second is via the change in the OOH_{ad} formation energy, which affects both k_{acid} and k_{base}.

While the electrolyte pH influences the OH_{ad} and O_{ad} adsorption in a way that preserves the scaling relation, the fact that the solvent affects the OH_{ad} and O_{ad} adsorption

DOI: 10.1021/jacs.6b11932
J. Am. Chem. Soc. 2017, 139, 3473−3479

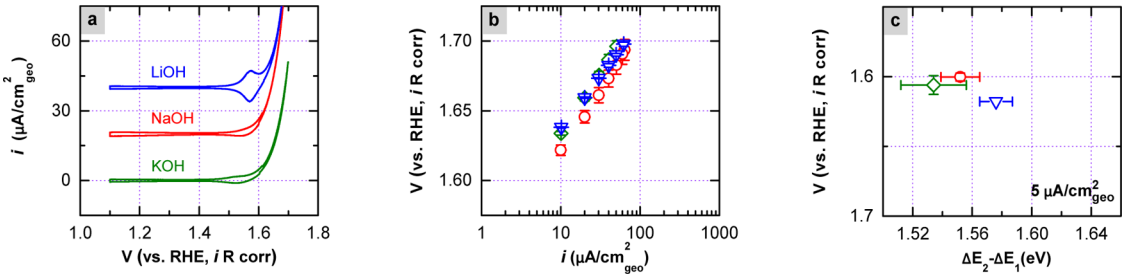

Figure 6. (a) Cyclic voltammograms of $IrO_2(110)$ in O_2-saturated 0.1 M KOH, NaOH, and LiOH at a scan rate of 10 mV/s. (b) Tafel plots for the OER kinetics of $IrO_2(110)$ in 0.1 M KOH, NaOH, and LiOH. (c) Overpotentials for the OER at 5 $\mu A/cm^2_{geo}$ in 0.1 M KOH, NaOH, and LiOH.

suggests a route to break it by controlling the interfacial water, for example, by way of changing the electrolyte cation. Figure 5a shows the CV curves of $IrO_2(110)$ in LiOH, NaOH, and KOH. We observe that the OH_{ad} adsorption shifts to a less positive potential while the O_{ad} adsorption shifts to a more positive potential in LiOH compared with KOH. Strmcnik and co-workers have reported that the OH_{ad} adsorption shifts to a less positive potential in LiOH because of the Li^+-OH_{ad} interaction, which stabilizes OH_{ad}.[71] We see a similar effect here. Notably, as shown in Figure 5c, the OH_{ad} adsorption energy becomes more favorable as we go from KOH to LiOH, while the O_{ad} adsorption energy is nearly independent of the electrolyte. This shift thus does not follow the scaling rule. We attribute this cation effect to the change in the structure of the surface water layer. Chu et al.[72] represented O_{ad} on $RuO_2(110)$ as being covered by an ice-like water monolayer. This water monolayer could reduce the interaction between cations and adsorbates, consequently causing the O_{ad} energy on IrO_2 to depend weakly on the cation.

Figure 6 shows the OER kinetics in 0.1 M KOH, NaOH, and LiOH. Interestingly, we observe that the activities of IrO_2 are similar in the three electrolytes, with the same Tafel slope. Unlike the pH dependence, the observed overpotential changes are not consistent with $\Delta E_2 - \Delta E_1$, a common OER descriptor for the formation of OOH_{ad} (Figure 6c). We hypothesize that this observation reflects the disruption of the scaling rule as a result of the interfacial water modification. This hypothesis, if correct, would suggest that the volcano relationship would no longer hold since the relations between the intermediates can be exploited by confining the water structure near the surface. Control of the activity using the confining electrocatalyst dimensionality as a tuning knob was recently reported by Vojvodic et al.[73]

CONCLUSIONS

We have reported the experimentally determined OH_{ad} and O_{ad} adsorption energies on $IrO_2(110)$ grown on $TiO_2(110)$ using MBE and linked the experimental surface adsorption to the OER kinetics. We have found that the energetics of the OER intermediates on $IrO_2(110)$ are not perfect but not too far off from the results of DFT calculations. It is likely that the solvent interactions at the electrochemical interface are the origin of this observed discrepancy. At higher pH, water dipoles stabilize the surface-adsorption, resulting in stronger adsorption, and we propose that this is due to the interaction between interfacial water and surface dipoles. This interaction preserves the scaling relation; however, the interaction between cations and adsorbates can disrupt it. We have further observed that the surface adsorption energy, as an outcome of the concept of the thermodynamic-limiting step, describes the OER kinetics for IrO_2 in acidic media. In alkaline media, however, the acid–base equilibrium causes the same mechanism to be dependent on OH^-, effectively causing the OER to stray from the volcano relationship. We have further demonstrated the use of different cations to tune the adsorption process in a way that does not follow the scaling relation. Our work establishes a link between surface adsorption energetics and OER electrocatalysis, provides adsorption benchmarks for future DFT calculations on transition-metal oxides, and highlights an opportunity to exploit the electrode–electrolyte interface for the design of future electrocatalysts.

ASSOCIATED CONTENT

Supporting Information

The Supporting Information is available free of charge on the ACS Publications website at DOI: 10.1021/jacs.6b11932.

Computational details, RHEED patterns of the $IrO_2(110)$ film, charge transfer density, OER activity at different pH values, and geometric models for DFT calculations (PDF)

AUTHOR INFORMATION

Corresponding Author

*jsuntivich@cornell.edu

ORCID

Geoffroy Hautier: 0000-0003-1754-2220

Jin Suntivich: 0000-0002-3427-4363

Present Address

⊥J.K.K.: Department of Materials Science and Engineering, University of Wisconsin—Madison, Madison, WI 53706, USA.

Notes

The authors declare no competing financial interest.

ACKNOWLEDGMENTS

We thank Ifan E. L Stephens for insightful discussions and for providing comments on the manuscript. Support for this work was provided by the Cornell Center for Materials Research under National Science Foundation (NSF) Grant DMR-1120296, part of the NSF MRSEC Program. J.K.K. acknowledges support from the Kavli Institute at Cornell for Nanoscience Science. J.N.N. acknowledges support from the NSF Graduate Research Fellowship under grant no. DGE-1650441. This work was performed in part at the Cornell NanoScale Facility (CNF), a member of the National Nanotechnology Infrastructure Network, which is supported by the NSF (Grant ECCS-0335765). Computational resources were provided by the Consortium des Équipements de Calcul

DOI: 10.1021/jacs.6b11932
J. Am. Chem. Soc. 2017, 139, 3473–3479

Intensif (CÉCI), funded by the Fonds de la Recherche Scientifique de Belgique (F.R.S.-FNRS) under Grant 2.5020.11.

REFERENCES

(1) Cook, T. R.; Dogutan, D. K.; Reece, S. Y.; Surendranath, Y.; Teets, T. S.; Nocera, D. G. *Chem. Rev.* **2010**, *110*, 6474.
(2) Hong, W. T.; Risch, M.; Stoerzinger, K. A.; Grimaud, A.; Suntivich, J.; Shao-Horn, Y. *Energy Environ. Sci.* **2015**, *8*, 1404.
(3) Bernt, M.; Gasteiger, H. A. *J. Electrochem. Soc.* **2016**, *163*, F3179.
(4) Fabbri, E.; Habereder, A.; Waltar, K.; Kötz, R.; Schmidt, T. J. *Catal. Sci. Technol.* **2014**, *4*, 3800.
(5) Koper, M. T. M. *J. Electroanal. Chem.* **2011**, *660*, 254.
(6) Man, I. C.; Su, H.-Y.; Calle-Vallejo, F.; Hansen, H. A.; Martínez, J. I.; Inoglu, N. G.; Kitchin, J.; Jaramillo, T. F.; Nørskov, J. K.; Rossmeisl, J. *ChemCatChem* **2011**, *3*, 1159.
(7) Rossmeisl, J.; Qu, Z.-W.; Zhu, H.; Kroes, G.-J.; Nørskov, J. K. *J. Electroanal. Chem.* **2007**, *607*, 83.
(8) Sabatier, P. *La Catalyse en Chimie Organique*; Béranger: Paris, 1920.
(9) Feng, Z. A.; Balaji Gopal, C.; Ye, X.; Guan, Z.; Jeong, B.; Crumlin, E.; Chueh, W. C. *Chem. Mater.* **2016**, *28*, 6233.
(10) Trasatti, S. *J. Electroanal. Chem. Interfacial Electrochem.* **1980**, *111*, 125.
(11) Suntivich, J.; Gasteiger, H. A.; Yabuuchi, N.; Nakanishi, H.; Goodenough, J. B.; Shao-Horn, Y. *Nat. Chem.* **2011**, *3*, 546.
(12) Nørskov, J. K.; Rossmeisl, J.; Logadottir, A.; Lindqvist, L.; Kitchin, J. R.; Bligaard, T.; Jonsson, H. *J. Phys. Chem. B* **2004**, *108*, 17886.
(13) Trotochaud, L.; Ranney, J. K.; Williams, K. N.; Boettcher, S. W. *J. Am. Chem. Soc.* **2012**, *134*, 17253.
(14) Suntivich, J.; May, K. J.; Gasteiger, H. A.; Goodenough, J. B.; Shao-Horn, Y. *Science* **2011**, *334*, 1383.
(15) Cheng, X.; Fabbri, E.; Nachtegaal, M.; Castelli, I. E.; El Kazzi, M.; Haumont, R.; Marzari, N.; Schmidt, T. J. *Chem. Mater.* **2015**, *27*, 7662.
(16) Petrie, J. R.; Cooper, V. R.; Freeland, J. W.; Meyer, T. L.; Zhang, Z.; Lutterman, D. A.; Lee, H. N. *J. Am. Chem. Soc.* **2016**, *138*, 2488.
(17) Grimaud, A.; May, K. J.; Carlton, C. E.; Lee, Y.-L.; Risch, M.; Hong, W. T.; Zhou, J.; Shao-Horn, Y. *Nat. Commun.* **2013**, *4*, 2439.
(18) Tang, R.; Nie, Y.; Kawasaki, J. K.; Kuo, D.-Y.; Petretto, G.; Hautier, G.; Rignanese, G.-M.; Shen, K. M.; Schlom, D. G.; Suntivich, J. *J. Mater. Chem. A* **2016**, *4*, 6831.
(19) Reier, T.; Pawolek, Z.; Cherevko, S.; Bruns, M.; Jones, T.; Teschner, D.; Selve, S.; Bergmann, A.; Nong, H. N.; Schlögl, R.; Mayrhofer, K. J. J.; Strasser, P. *J. Am. Chem. Soc.* **2015**, *137*, 13031.
(20) Nong, H. N.; Oh, H.-S.; Reier, T.; Willinger, E.; Willinger, M.-G.; Petkov, V.; Teschner, D.; Strasser, P. *Angew. Chem., Int. Ed.* **2015**, *54*, 2975.
(21) Kim, J.; Yin, X.; Tsao, K.-C.; Fang, S.; Yang, H. *J. Am. Chem. Soc.* **2014**, *136*, 14646.
(22) Rossmeisl, J.; Nørskov, J. K.; Taylor, C. D.; Janik, M. J.; Neurock, M. *J. Phys. Chem. B* **2006**, *110*, 21833.
(23) Sheng, W.; Zhuang, Z.; Gao, M.; Zheng, J.; Chen, J. G.; Yan, Y. *Nat. Commun.* **2015**, *6*, 5848.
(24) Zheng, J.; Sheng, W.; Zhuang, Z.; Xu, B.; Yan, Y. *Sci. Adv.* **2016**, *2*, e1501602.
(25) van der Niet, M. J. T. C.; Dominicus, I.; Koper, M. T. M.; Juurlink, L. B. F. *Phys. Chem. Chem. Phys.* **2008**, *10*, 7169.
(26) van der Niet, M. J. T. C.; den Dunnen, A.; Juurlink, L. B. F.; Koper, M. T. M. *Phys. Chem. Chem. Phys.* **2011**, *13*, 1629.
(27) Zhang, Z.; Fenter, P.; Cheng, L.; Sturchio, N. C.; Bedzyk, M. J.; Předota, M.; Bandura, A.; Kubicki, J. D.; Lvov, S. N.; Cummings, P. T.; Chialvo, A. A.; Ridley, M. K.; Bénézeth, P.; Anovitz, L.; Palmer, D. A.; Machesky, M. L.; Wesolowski, D. J. *Langmuir* **2004**, *20*, 4954.
(28) Nakagawa, N.; Hwang, H. Y.; Muller, D. A. *Nat. Mater.* **2006**, *5*, 204.
(29) Watanabe, E.; Rossmeisl, J.; Björketun, M. E.; Ushiyama, H.; Yamashita, K. *J. Phys. Chem. C* **2016**, *120*, 8096.
(30) Gómez-Marín, A. M.; Rizo, R.; Feliu, J. M. *Beilstein J. Nanotechnol.* **2013**, *4*, 956.
(31) Gomez, R.; Orts, J. M.; Alvarez-Ruiz, B.; Feliu, J. M. *J. Phys. Chem. B* **2004**, *108*, 228.
(32) Bandarenka, A. S.; Hansen, H. A.; Rossmeisl, J.; Stephens, I. E. L. *Phys. Chem. Chem. Phys.* **2014**, *16*, 13625.
(33) Hoster, H. E.; Alves, O. B.; Koper, M. T. M. *ChemPhysChem* **2010**, *11*, 1518.
(34) McCrum, I. T.; Janik, M. J. *J. Phys. Chem. C* **2016**, *120*, 457.
(35) Karlberg, G. S.; Jaramillo, T. F.; Skúlason, E.; Rossmeisl, J.; Bligaard, T.; Nørskov, J. K. *Phys. Rev. Lett.* **2007**, *99*, 126101.
(36) Stamenkovic, V. R.; Fowler, B.; Mun, B. S.; Wang, G.; Ross, P. N.; Lucas, C. A.; Markovic, N. M. *Science* **2007**, *315*, 493.
(37) Greeley, J.; Stephens, I. E. L.; Bondarenko, A. S.; Johansson, T. P.; Hansen, H. A.; Jaramillo, T. F.; Rossmeisl, J.; Chorkendorff, I.; Nørskov, J. K. *Nat. Chem.* **2009**, *1*, 552.
(38) Liang, T.; Koohpayeh, S. M.; Krizan, J. W.; McQueen, T. M.; Cava, R. J.; Ong, N. P. *Nat. Commun.* **2015**, *6*, 7611.
(39) O'Grady, W. E.; Goel, A. K.; Pollak, F. H.; Park, H. L.; Huang, Y. S. *J. Electroanal. Chem. Interfacial Electrochem.* **1983**, *151*, 295.
(40) Castelli, P.; Trasatti, S.; Pollak, F. H.; O'Grady, W. E. *J. Electroanal. Chem. Interfacial Electrochem.* **1986**, *210*, 189.
(41) Hepel, T.; Pollak, F. H.; O'Grady, W. E. *J. Electrochem. Soc.* **1984**, *131*, 2094.
(42) Hepel, T.; Pollak, F. H.; O'Grady, W. E. *J. Electrochem. Soc.* **1985**, *132*, 2385.
(43) Stoerzinger, K. A.; Qiao, L.; Biegalski, M. D.; Shao-Horn, Y. *J. Phys. Chem. Lett.* **2014**, *5*, 1636.
(44) Stoerzinger, K. A.; Choi, W. S.; Jeen, H.; Lee, H. N.; Shao-Horn, Y. *J. Phys. Chem. Lett.* **2015**, *6*, 487.
(45) Tkatchenko, A.; Scheffler, M. *Phys. Rev. Lett.* **2009**, *102*, 073005.
(46) Hammer, B.; Hansen, L. B.; Nørskov, J. K. *Phys. Rev. B: Condens. Matter Mater. Phys.* **1999**, *59*, 7413.
(47) Hansen, H. A.; Man, I. C.; Studt, F.; Abild-Pedersen, F.; Bligaard, T.; Rossmeisl, J. *Phys. Chem. Chem. Phys.* **2010**, *12*, 283.
(48) Kresse, G.; Hafner, J. *Phys. Rev. B: Condens. Matter Mater. Phys.* **1993**, *47*, 558.
(49) Kresse, G.; Furthmüller, J. *Phys. Rev. B: Condens. Matter Mater. Phys.* **1996**, *54*, 11169.
(50) Kresse, G.; Furthmüller, J. *Comput. Mater. Sci.* **1996**, *6*, 15.
(51) Blum, V.; Gehrke, R.; Hanke, F.; Havu, P.; Havu, V.; Ren, X.; Reuter, K.; Scheffler, M. *Comput. Phys. Commun.* **2009**, *180*, 2175.
(52) Kresse, G.; Joubert, D. *Phys. Rev. B: Condens. Matter Mater. Phys.* **1999**, *59*, 1758.
(53) Mathew, K.; Sundararaman, R.; Letchworth-Weaver, K.; Arias, T. A.; Hennig, R. G. *J. Chem. Phys.* **2014**, *140*, 084106.
(54) Mathew, K.; Hennig, R. G. Implicit self-consistent description of electrolyte in plane-wave density-functional theory. 2016, arXiv:1601.03346. arXiv.org e-Print archive. http://arxiv.org/abs/1601.03346 (accessed Nov 17, 2016).
(55) Kawasaki, J. K.; Uchida, M.; Paik, H.; Schlom, D. G.; Shen, K. M. *Phys. Rev. B: Condens. Matter Mater. Phys.* **2016**, *94*, 121104.
(56) Blakemore, J. D.; Schley, N. D.; Kushner-Lenhoff, M. N.; Winter, A. M.; D'Souza, F.; Crabtree, R. H.; Brudvig, G. W. *Inorg. Chem.* **2012**, *51*, 7749.
(57) Mo, Y.; Stefan, I. C.; Cai, W.-B.; Dong, J.; Carey, P.; Scherson, D. A. *J. Phys. Chem. B* **2002**, *106*, 3681.
(58) Hüppauff, M. *J. Electrochem. Soc.* **1993**, *140*, 598.
(59) Pauporté, T.; Aberdam, D.; Hazemann, J. L.; Faure, R.; Durand, R. *J. Electroanal. Chem.* **1999**, *465*, 88.
(60) Viswanathan, V.; Hansen, H. A.; Rossmeisl, J.; Jaramillo, T. F.; Pitsch, H.; Nørskov, J. K. *J. Phys. Chem. C* **2012**, *116*, 4698.
(61) Burke, L. D.; Mulcahy, J. K.; Whelan, D. P. *J. Electroanal. Chem. Interfacial Electrochem.* **1984**, *163*, 117.
(62) Steegstra, P.; Busch, M.; Panas, I.; Ahlberg, E. *J. Phys. Chem. C* **2013**, *117*, 20975.
(63) Schwarz, K.; Xu, B.; Yan, Y.; Sundararaman, R. *Phys. Chem. Chem. Phys.* **2016**, *18*, 16216.

DOI: 10.1021/jacs.6b11932
J. Am. Chem. Soc. 2017, 139, 3473−3479

(64) van der Niet, M. J. T. C.; Garcia-Araez, N.; Hernández, J.; Feliu, J. M.; Koper, M. T. M. *Catal. Today* **2013**, *202*, 105.
(65) Gisbert, R.; García, G.; Koper, M. T. M. *Electrochim. Acta* **2010**, *55*, 7961.
(66) Fernández, E. M.; Moses, P. G.; Toftelund, A.; Hansen, H. A.; Martínez, J. I.; Abild-Pedersen, F.; Kleis, J.; Hinnemann, B.; Rossmeisl, J.; Bligaard, T.; Nørskov, J. K. *Angew. Chem.* **2008**, *120*, 4761.
(67) Hansen, M. H.; Rossmeisl, J. *J. Phys. Chem. C* **2016**, *120*, 29135.
(68) Lee, Y.; Suntivich, J.; May, K. J.; Perry, E. E.; Shao-Horn, Y. *J. Phys. Chem. Lett.* **2012**, *3*, 399.
(69) Minguzzi, A.; Fan, F.-R. F.; Vertova, A.; Rondinini, S.; Bard, A. J. *Chem. Sci.* **2012**, *3*, 217.
(70) Goodenough, J. B.; Manoharan, R.; Paranthaman, M. *J. Am. Chem. Soc.* **1990**, *112*, 2076.
(71) Strmcnik, D.; Kodama, K.; van der Vliet, D.; Greeley, J.; Stamenkovic, V. R.; Marković, N. M. *Nat. Chem.* **2009**, *1*, 466.
(72) Chu, Y. S.; Lister, T. E.; Cullen, W. G.; You, H.; Nagy, Z. *Phys. Rev. Lett.* **2001**, *86*, 3364.
(73) Doyle, A. D.; Montoya, J. H.; Vojvodic, A. *ChemCatChem* **2015**, *7*, 738.

DOI: 10.1021/jacs.6b11932
J. Am. Chem. Soc. 2017, 139, 3473−3479